

Updated global fit to three neutrino mixing: status of the hints of $\theta_{13} > 0$

M. C. Gonzalez-Garcia

*C.N. Yang Institute for Theoretical Physics
State University of New York at Stony Brook
Stony Brook, NY 11794-3840, USA,
and: Institució Catalana de Recerca i Estudis Avançats (ICREA),
Departament d'Estructura i Constituents de la Matèria and Institut de Ciències del
Cosmos, Universitat de Barcelona, Diagonal 647, E-08028 Barcelona, Spain
E-mail: concha@insti.physics.sunysb.edu*

Michele Maltoni

*Instituto de Física Teórica UAM/CSIC, Facultad de Ciencias, Universidad Autónoma
de Madrid, Cantoblanco, E-28049 Madrid, Spain
E-mail: michele.maltoni@uam.es*

Jordi Salvado

*Departament d'Estructura i Constituents de la Matèria and Institut de Ciències del
Cosmos, Universitat de Barcelona, 647 Diagonal, E-08028 Barcelona, Spain
E-mail: jsalvado@ecm.ub.es*

ABSTRACT: We present an up-to-date global analysis of solar, atmospheric, reactor and accelerator neutrino data in the framework of three-neutrino oscillations. We discuss in detail the statistical significance of the observed “hint” of non-zero θ_{13} in the solar sector at the light of the latest experimental advances, such as the Borexino spectral data, the lower value of Gallium rate recently measured in SAGE, and the low energy threshold analysis of the combined SNO phase I and phase II. We also study the robustness of the results under changes of the inputs such as the choice of solar model fluxes and a possible modification of the Gallium capture cross-section as proposed by SAGE. In the atmospheric sector we focus on the latest results for ν_e appearance from MINOS, and we discuss their impact on the determination of θ_{13} . Finally, we combine all the data into a global analysis and determine the presently allowed ranges of masses and mixing.

KEYWORDS: neutrino oscillations, solar and atmospheric neutrinos.

Contents

1. Introduction	1
2. Leading Δm_{21}^2 oscillations: solar and KamLAND data	2
2.1 Impact of θ_{13} on the solar analysis	6
2.2 Combination with KamLAND and the hint of $\theta_{13} \neq 0$	8
3. Leading Δm_{31}^2 oscillations: atmospheric, CHOOZ and accelerator data	10
3.1 Impact of θ_{13} on the atmospheric and LBL ν_μ disappearance data	11
3.2 $\nu_\mu \rightarrow \nu_e$ appearance results in MINOS	12
4. Global results and conclusions	13

1. Introduction

It is now an established fact that neutrinos are massive and leptonic flavors are not symmetries of Nature [1, 2]. In the last decade this picture has become fully proved thanks to the upcoming of a set of precise experiments. In particular, the results obtained with solar and atmospheric neutrinos have been confirmed in experiments using terrestrial beams: neutrinos produced in nuclear reactors and accelerators facilities have been detected at distances of the order of hundreds of kilometers [3].

The minimum joint description of all the neutrino data requires mixing among all the three known neutrinos (ν_e, ν_μ, ν_τ), which can be expressed as quantum superpositions of three massive states ν_i ($i = 1, 2, 3$) with masses m_i . This implies the presence of a leptonic mixing matrix in the weak charged current interactions [4, 5] which can be parametrized as:

$$U = \begin{pmatrix} c_{12}c_{13} & s_{12}c_{13} & s_{13}e^{-i\delta_{\text{CP}}} \\ -s_{12}c_{23} - c_{12}s_{13}s_{23}e^{i\delta_{\text{CP}}} & c_{12}c_{23} - s_{12}s_{13}s_{23}e^{i\delta_{\text{CP}}} & c_{13}s_{23} \\ s_{12}s_{23} - c_{12}s_{13}c_{23}e^{i\delta_{\text{CP}}} & -c_{12}s_{23} - s_{12}s_{13}c_{23}e^{i\delta_{\text{CP}}} & c_{13}c_{23} \end{pmatrix}, \quad (1.1)$$

where $c_{ij} \equiv \cos \theta_{ij}$ and $s_{ij} \equiv \sin \theta_{ij}$. In addition to the Dirac-type phase δ_{CP} , analogous to that of the quark sector, there are two physical phases associated to the Majorana character of neutrinos, which however are not relevant for neutrino oscillations [6, 7] and are therefore omitted on the present work. Given the observed hierarchy between the solar and atmospheric mass-squared splittings there are two possible non-equivalent orderings for the mass eigenvalues, which are conventionally chosen as

$$\Delta m_{21}^2 \ll (\Delta m_{32}^2 \simeq \Delta m_{31}^2 > 0); \quad (1.2)$$

$$\Delta m_{21}^2 \ll -(\Delta m_{31}^2 \simeq \Delta m_{32}^2 < 0). \quad (1.3)$$

As it is customary we refer to the first option, Eq. (1.2), as the *normal* scheme, and to the second one, Eq. (1.3), as the *inverted* scheme; in this form they correspond to the two possible choices of the sign of Δm_{31}^2 . In this convention the angles θ_{ij} can be taken without loss of generality to lie in the first quadrant, $\theta_{ij} \in [0, \pi/2]$, and the CP phase $\delta_{\text{CP}} \in [0, 2\pi]$.

Within this context, Δm_{21}^2 , $|\Delta m_{31}^2|$, θ_{12} , and θ_{23} are relatively well determined [3, 8–10], while only an upper bound is derived for the mixing angle θ_{13} and barely nothing is known on the CP phase δ_{CP} and on the sign of Δm_{31}^2 . Apart from the importance from a theoretical point of view, establishing whether θ_{13} is zero or not is an essential step in the development of the search strategies for the upcoming experiments. Once we know that the two mixing angles θ_{12} and θ_{23} are relatively large, the possibility of experimentally accessing leptonic CP violation crucially depends on the value of the angle θ_{13} . Also a non-zero θ_{13} is a fundamental ingredient for a feasible determination of the neutrino mass ordering. For this reason, it is a main objective of upcoming reactor and accelerator experiments to directly measure this parameter. In this respect, Refs. [11, 12] pointed out that two independent hints in favor of a non-zero value of θ_{13} emerge from the combination of solar and long-baseline (LBL) reactor data as well as from the combination of atmospheric, short-baseline reactor and LBL accelerator data. Since these signals are the results of synergies between different data samples, it is particularly important to verify their stability with respect to new experimental data as well as to variations on the assumptions in the analysis.

In this work we present the results of an up-to-date global analysis of solar, atmospheric, reactor and LBL accelerator neutrino data in the context of three-neutrino oscillations. In Sec. 2 we focus on the solar sector and we assess the stability of the oscillation parameters with respect to the inclusion of the new experimental results and theoretical advances which have become public during the last year. In this context, we find that many of these changes indeed lower the statistical significance of a non-zero value of θ_{13} . In Sec. 3 we do the same in the atmospheric sector, with particular emphasis on the recent ν_e appearance results from MINOS. In Sec. 4 we combine all the data together and we determine the presently allowed ranges of mass and mixing, thus updating our previous results.

2. Leading Δm_{21}^2 oscillations: solar and KamLAND data

In the analysis of solar neutrino experiments we include the total rates from the radiochemical experiments Chlorine [18], Gallex/GNO [19] and SAGE [13]. For real-time experiments we include the 44 data points of the electron scattering (ES) Super-Kamiokande phase I (SK-I) energy-zenith spectrum [20] and the data from the three phases of SNO [21–23], including the results on the low energy threshold analysis of the combined SNO phase I and phase II [16] (which we label SNO-LETA). We also include the main set of the 192 days of Borexino data [14] (which we label Borexino-LE) as well as their high-energy spectrum from 246 live days [15] (Borexino-HE). We consider the following variations on the analysis:

- **Updated capture rate in gallium.** In Ref. [13] the Russian-American experiment SAGE has presented the results of the combined analysis of 168 extractions (until

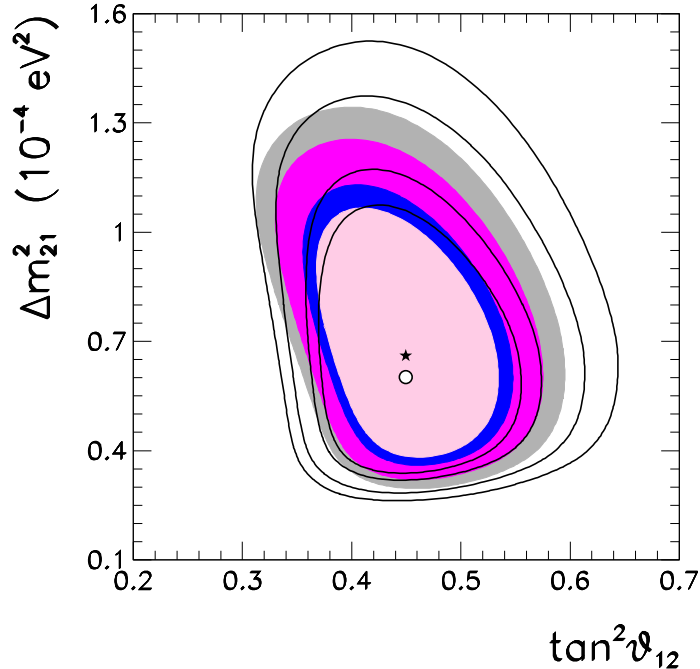


Figure 1: Allowed parameter regions (at 90%, 95%, 99% and 99.73% CL for 2 d.o.f.) from the combined analysis of solar data for $\theta_{13} = 0$. The best fit point is marked with a star. For comparison we also show as empty regions (the best fit is marked by a circle) the results prior to the inclusion of the latest Ga capture rate of SAGE [13], the energy spectrum of Borexino [14, 15] and the low energy threshold analysis of the combined SNO phase I and phase II [16]. In both analysis we use as inputs the GS98 solar model fluxes and the Gallium capture cross-section of Bahcall [17].

December 2007). The capture rate of solar neutrinos above the 233 keV threshold is

$$R_{\text{SAGE}}^{09} = 65.4_{-3.0}^{+3.1} (\text{stat})_{-2.8}^{+2.6} (\text{syst}) \text{ SNU}. \quad (2.1)$$

which is slightly lower (but fully consistent) than the previous result quoted in Ref. [19], $66.2_{-3.2}^{+3.3} (\text{stat})_{-3.2}^{+3.5} (\text{syst}) \text{ SNU}$, and presents a considerable improvement of the systematic uncertainties.

- **Possible modification of the capture cross-section in gallium.** Ref. [13] also presents the results of a new calibration of the SAGE detector with a reactor-produced ^{37}Ar neutrino source. The ratio of observed to expected event rate in this experiment, once combined with the measured rates in the three prior ^{51}Cr neutrino-source experiments with Gallium, is 0.87 ± 0.05 . As a possible explanation for this low result, in Ref. [13] it is proposed that the the cross-section for neutrino capture by the two lowest-lying excited states in ^{71}Ge may have been overestimated in Ref. [17]. As an alternative, the authors consider a modified capture cross-section where the contribution from these two excited states is set to zero.
- **Inclusion of the Borexino spectral data.** Following the procedure described in Ref. [24] (see Appendix A of that work for details) we have included in the analysis

the 160 data points of the Borexino energy spectrum in the 365–2000 keV energy range [14] as well as the 7 points of the high-energy spectrum from the 246 live days of Borexino [15]. In our approach the overall normalizations of the ^{11}C , ^{14}C , ^{210}Bi and ^{85}Kr backgrounds are introduced as free parameters and are fitted to the data.

- **Low energy threshold analysis of the combined SNO phase I and phase II data.** In Ref. [16] the SNO Collaboration reported the results from a joint analysis of their Phase I and Phase II data with an effective electron kinetic energy threshold of $T_{\text{eff}} = 3.5$ MeV. Besides the inclusion of the lower energy data the analysis present improvements in the calibration and analysis techniques to reduce the threshold and increase the precision of the results.

From the point of view of any reanalysis of their data, there is an important difference with respect to the previous higher threshold results. In Refs. [21,22] the results were quoted in the form of binned (in energy and time) event rates. In particular, 34 data points of the day-night spectrum were given for SNO-I, and the separate day and night rates for neutral current (NC) and ES events as well as the day-night energy-spectrum for charge current (CC) events were given for SNO-II. Instead, in Ref. [16] the collaboration presents its reanalysis as a total ^8B neutrino flux plus an effective description (under the assumption of unitarity for active neutrinos) of the ν_e survival probability, whose dependence on E_ν is parametrized as a quadratic function for P_{ee}^{day} and a linear function for the day/night asymmetry. In other words, the SNO-LETA results are given as best fit, uncertainties and correlations of six effective parameters: the ^8B flux, three polynomial coefficients of E_ν for the P_{ee}^{day} and two for the day-night asymmetry. When using these data to perform a fit to neutrino oscillations, for each value of the oscillation parameters one must first obtain the polynomial coefficients that best represent the corresponding MSW [25, 26] oscillation probability. This has to be done taking into account the sensitivity of the SNO detector, and the relevant information is provided in the Appendix A of Ref. [16]. We have followed the procedure outlined there and we have verified that we can perfectly reproduce their oscillation results in Fig. 37.¹

- **Uncertainties on the Solar Model.** Recent detailed determination of the abundances of the heavy elements on the solar surface [27,28] lead to lower values than previous studies [29]. Any solar model which incorporates such lower metallicities fails at explaining the helioseismological observations [30]. Changes in the Sun modeling, in particular of the less known convective zone, are not able to account for this discrepancy [31,32]. So far there has not been a successful solution of this puzzle, so that at present there is no fully consistent Standard Solar Model (SSM). This lead to the construction of two different sets of SSM's, one (labeled “GS”) based on the older

¹However we notice that this procedure does not allow the inclusion of the SNO low energy threshold data in analysis in terms of more exotic scenarios in which either unitarity in the active neutrino sector does not hold (like for scenarios with sterile neutrinos) or the energy dependence of the oscillation probability cannot be well represented by a simple quadratic function.

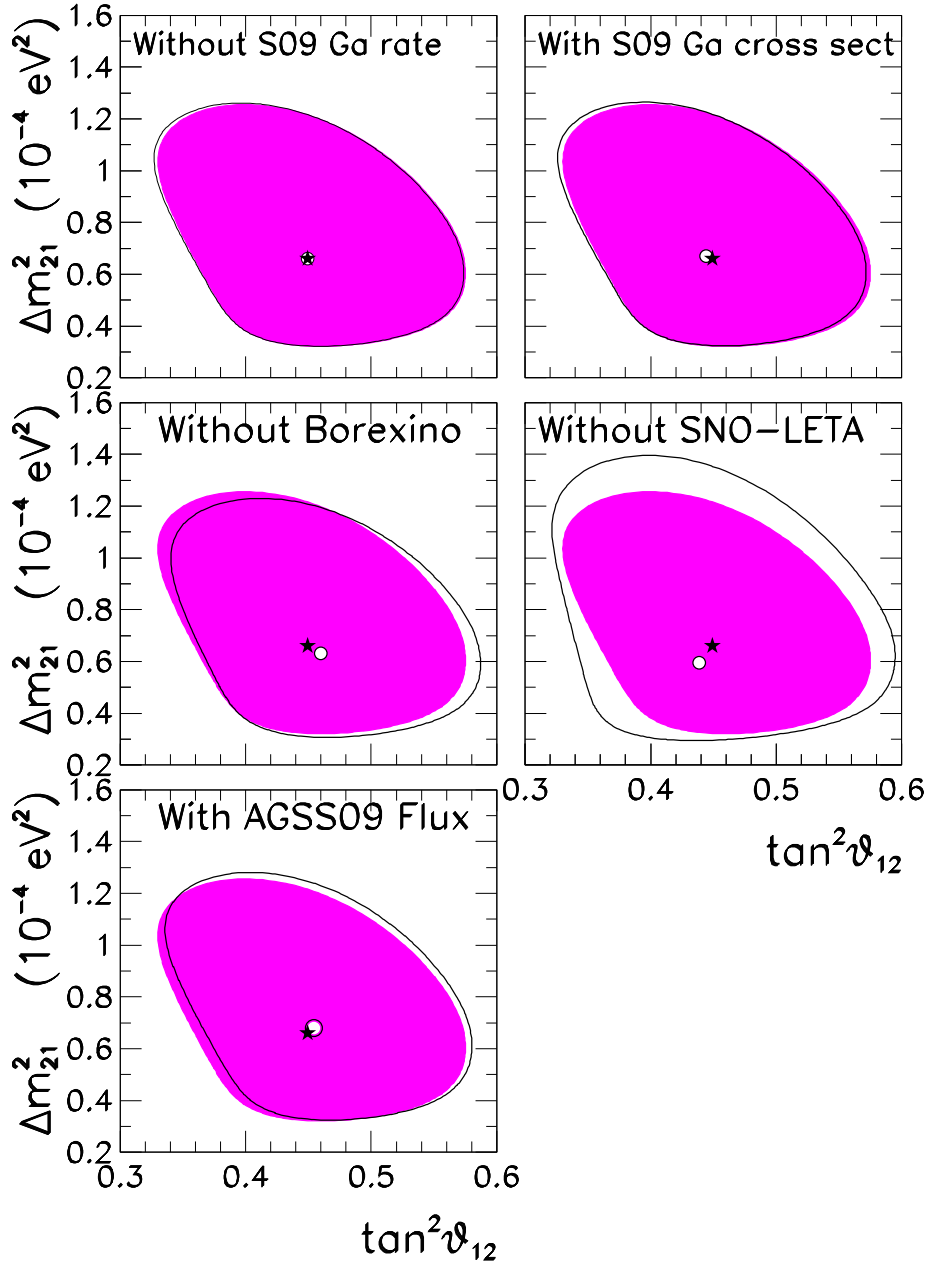


Figure 2: Effects of the different assumed inputs on the 99% CL parameter region from the combined analysis of solar data for $\theta_{13} = 0$. The full region corresponds to the results show in Fig. 1. The solid line corresponds to the modification due to the change on one of the inputs as labeled in each panel.

solar abundances [29] leading to high metallicity, and one (labeled “AGS”) assuming lower metallicity [33]. We use the most recent recalculation of the fluxes in these two sets from Ref. [34], and following their notation we refer to them as GS98 and AGSS09.

Let us first consider the case $\theta_{13} = 0$. In Fig. 1 we show the present determination of the

leading parameters Δm_{21}^2 and θ_{12} from the updated oscillation analysis of the solar neutrino data described above in the context of the GS98 solar model. For comparison we also show the results obtained prior to the inclusion of the latest Ga capture rate of SAGE [13], the energy spectrum of Borexino [14, 15] and the SNO-LETA results [16] for the same solar model. As seen in this figure, the inclusion of these results lead to an improvement on the determination of both θ_{12} and Δm_{21}^2 and for this last one the best fit value slightly increases. The effect of the different variations in the analysis is displayed in Fig. 2, where we show the 99% CL region in the $(\Delta m_{21}^2, \tan^2 \theta_{12})$ plane from the present analysis and the corresponding one when some of the input data or assumption are modified. The figure shows that the most quantitatively relevant new information arises from the inclusion of the SNO-LETA results. The inclusion of Borexino tends to shift the region towards slightly lower values of θ_{12} angle. Conversely, if the analysis is done in the context of the AGSS09 model the region is shifted towards slightly larger θ_{12} .

2.1 Impact of θ_{13} on the solar analysis

The survival probability of solar neutrinos in the framework of three neutrino oscillations can be written as:

$$P_{ee}^{3\nu} = \sin^4 \theta_{13} + \cos^4 \theta_{13} P_{ee}^{2\nu}(\Delta m_{21}^2, \theta_{12}), \quad (2.2)$$

where we have used the fact that $L_{31}^{\text{osc}} = 4\pi E/\Delta m_{31}^2$ is much shorter than the distance between the Sun and the Earth, so that the oscillations related to L_{31}^{osc} are averaged. In presence of matter effects $P_{ee}^{2\nu}(\Delta m_{21}^2, \theta_{12})$ should be calculated taking into account the evolution in an effective matter density $n_e^{\text{eff}} = n_e \cos^2 \theta_{13}$. For $10^{-5} \lesssim \Delta m^2/\text{eV}^2 \lesssim 10^{-4}$, $P_{ee}^{2\nu}(\Delta m_{21}^2, \theta_{12})$ presents the following asymptotic behaviors:

$$P_{ee}^{2\nu}(\Delta m_{21}^2, \theta_{12}) \simeq 1 - \frac{1}{2} \sin^2(2\theta_{12}) \quad \text{for } E_\nu \lesssim \text{few} \times 100 \text{ KeV} \quad (2.3)$$

$$P_{ee}^{2\nu}(\Delta m_{21}^2, \theta_{12}) \simeq \sin^2(\theta_{12}) \quad \text{for } E_\nu \gtrsim \text{few} \times 1 \text{ MeV} \quad (2.4)$$

The impact of the inclusion of a non-zero value of θ_{13} in the solar analysis is shown in Fig. 3 and in the upper-left panel of Fig. 4. From this last plot we see that solar neutrino data by themselves favor $\theta_{13} = 0$, although their sensitivity is very weak for $\sin^2 \theta_{13} \lesssim 0.03$. This behavior can be understood from Fig. 3, where we show the allowed regions (at 95% CL) in the $(\Delta m_{21}^2, \tan^2 \theta_{12})$ plane as obtained from the analysis of low-energy (radiochemical and Borexino-LE) and high-energy (SK, SNO and Borexino-HE) solar experiments, for different values of θ_{13} . As described in Eq. (2.2), for fixed values of Δm_{21}^2 and θ_{12} , the inclusion of a small value of θ_{13} results into a decrease on the predicted rates at a given solar neutrino experiment. This decrease can be compensated by a shift of Δm_{21}^2 and θ_{12} which lead to an increase of $P_{ee}^{2\nu}$. However the sign of the shift strongly depends on the characteristic energy of the detected neutrinos. For experiments detecting neutrinos with energies low enough for matter effects to be irrelevant (such as Chlorine and Gallium experiments) $P_{ee}^{2\nu}$ is given by Eq. (2.3) and increases as θ_{12} decreases. Conversely, for experiments detecting neutrinos mostly in the regime of adiabatic matter oscillations (such as SK and SNO) $P_{ee}^{2\nu}$ is given by Eq. (2.4) and increases as θ_{12} increases. Consequently the combined fit worsens with θ_{13} .

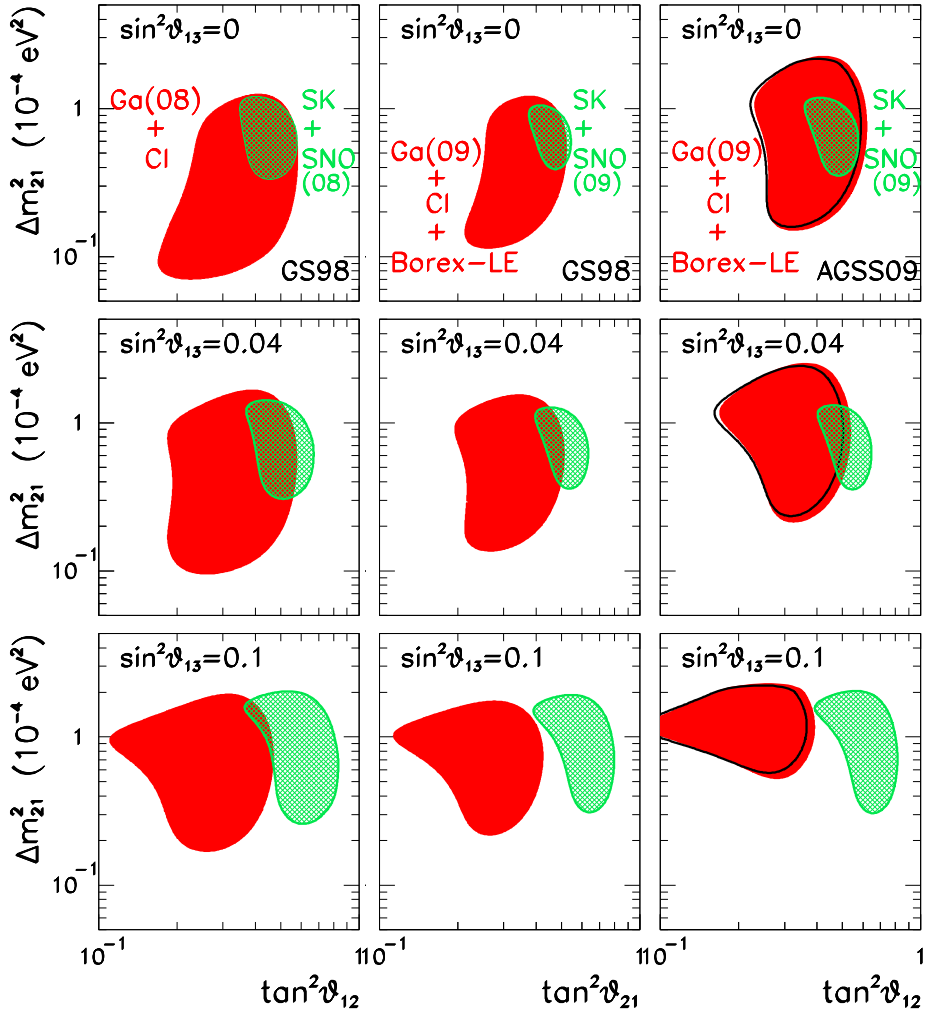


Figure 3: Dependence on θ_{13} of the allowed $(\Delta m_{21}^2, \tan^2 \theta_{12})$ regions (at 95% CL for 2 d.o.f.) from the partial analysis of the “low energy” and “high energy” solar neutrino data. The left column corresponds to the analysis prior to the inclusion of the latest Ga capture rate of SAGE [13], the energy spectrum of Borexino [14, 15] and the low energy threshold analysis of the combined SNO phase I and phase II [16]. In the central and right columns the results of those experiments are included. The central column corresponds to GS98 solar model fluxes and Gallium capture cross-section of Bahcall [17]. In the right panels the AGSS09 solar model fluxes are used. The full (void) regions are obtained with Gallium capture cross-section of Bahcall [17] (modified cross-section in Ref. [13]).

Fig. 3 also illustrates how the inclusion of the new data strengthens this tension. The quantitative improvement on the corresponding bound on θ_{13} is displayed in the upper-left panel of Fig. 4. We have also studied the dependence of this result on the assumed solar model and on the possible modification of the neutrino capture in gallium. We find that the AGSS09 fluxes lead to a stronger bound on θ_{13} and the same happens with the modified gallium cross-section. This second effect can be easily understood as follows: because of the lower cross-section, a slightly larger survival probability is required to fit the same

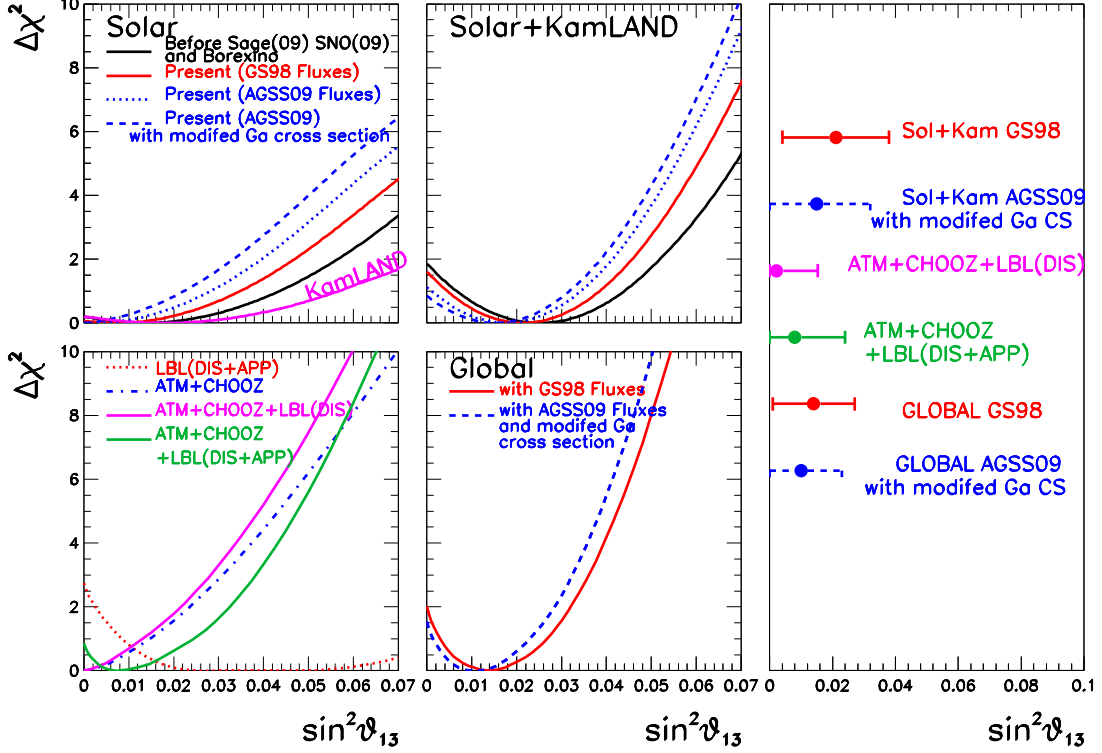


Figure 4: Dependence of $\Delta\chi^2$ on $\sin^2\theta_{13}$ for the different analysis as labeled in the figure and the corresponding 1σ ranges.

data. This shifts the $(\Delta m_{21}^2, \tan^2\theta_{12})$ allowed region obtained from the analysis of the radiochemical solar experiments towards slightly lower values of θ_{12} (as explicitly shown in the last column of Fig. 3). As a consequence it increases the tension with the SNO+SK favored mixing angle for non-zero θ_{13} .

2.2 Combination with KamLAND and the hint of $\theta_{13} \neq 0$

We show in the left panels of Fig. 5 the present determination of the leading parameters Δm_{21}^2 and θ_{12} (for $\theta_{13} = 0$) from the analysis of KamLAND spectral data [35] compared to those from the updated solar analysis for the two solar models considered. While the results show perfect agreement in Δm_{21}^2 , there appears to be a mismatch in the favored value of θ_{12} as determined from KamLAND compared to the one from solar neutrinos, this last one being mostly sensitive to the precise value of CC/NC event (*i.e.*, to $\langle P_{ee} \rangle \propto \sin^2\theta_{12}$) as determined by SK and SNO.

As it was pointed out in Ref. [11] and widely discussed in the literature [8–10], this mismatch can be lifted by a non-zero value of θ_{13} . This happens because, as discussed above, the CC/NC event rate can be fitted with a higher value of θ_{12} provided that a non-zero θ_{13} is included. Conversely for KamLAND Eq. (2.2) also holds with

$$P_{ee}^{2\nu, \text{kam}} = 1 - \frac{1}{2} \sin^2(2\theta_{12}) \sin^2 \frac{\Delta m_{21}^2 L}{2E}. \quad (2.5)$$

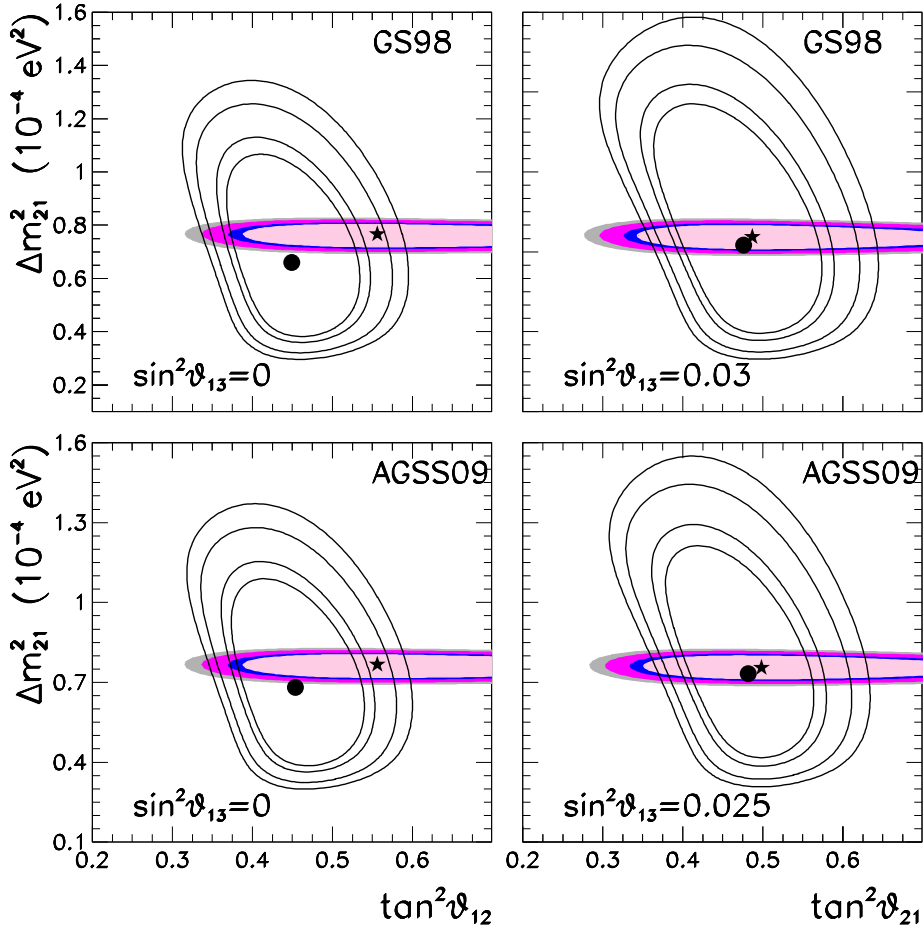


Figure 5: Allowed parameter regions (at 90%, 95%, 99% and 99.73% CL for 2 d.o.f.) from analysis of KamLAND (full regions with best fit marked by a star) and solar (void regions with best fit marked by a dot) data for two values of θ_{13} as labeled in the figure and for the two solar models.

So for $\theta_{13} > 0$ the KamLAND spectrum can be well fitted with a smaller value of θ_{12} , and consequently the best fit values for solar and KamLAND analysis agree better for $\theta_{13} \neq 0$. This behavior is clearly visible in the right panels of Fig. 5 and in the upper-central panel of Fig. 4. As mentioned before, the best fit value of θ_{12} for solar neutrino fit within the AGSS09 model is slightly larger than for the GS98 model, and therefore the required value of θ_{13} to achieve agreement with KamLAND is smaller for the AGSS09 model.

However, one must notice that the better agreement between the solar and KamLAND analysis for $\theta_{13} \neq 0$ has to be contrasted with the worsening of the global description of the solar neutrino data previously described. As a consequence of this tension we find that the inclusion of the new data and of the modified gallium capture cross-section also tend to lower the best fit value of θ_{13} as well as its corresponding statistical significance (see upper-central panel of Fig. 4). Altogether we find that the 1σ range for θ_{13} as determined from the global analysis of solar and KamLAND data changes from the old value $\sin^2 \theta_{13} =$

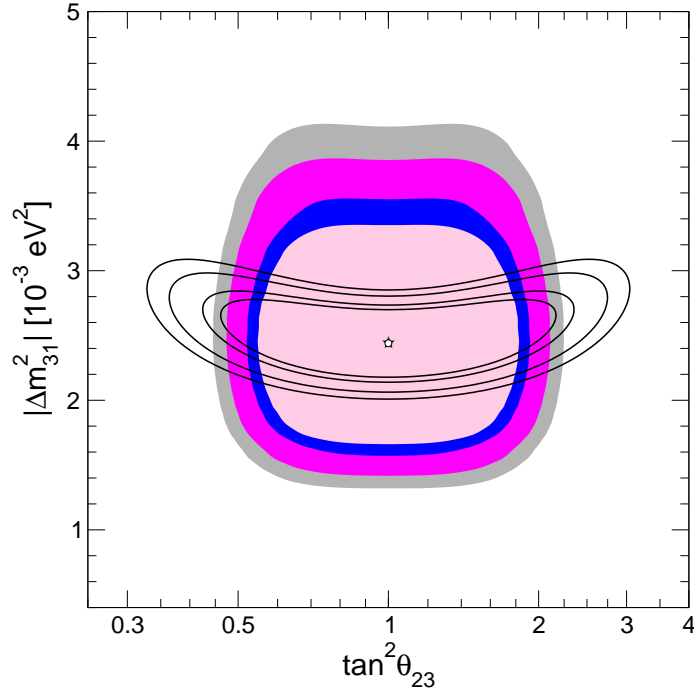


Figure 6: Allowed parameter regions (at 90%, 95%, 99% and 99.73% CL for 2 d.o.f.) from the analysis of atmospheric data (full regions, best fit marked with a star) and LBL data (void regions and best fit marked by a circle) for $\theta_{13} = 0$ and $\Delta m_{21}^2 = 0$.

0.025 ± 0.018 (before the inclusion of SNO-LETA, SAGE-09 and Borexino data) to:

$$\sin^2 \theta_{13} = \begin{cases} 0.021 \pm 0.017 & \text{for GS98,} \\ 0.017 \pm 0.017 & \text{for AGSS09,} \\ 0.015 \pm 0.017 & \text{for AGSS09 with modified Ga cross-section.} \end{cases} \quad (2.6)$$

3. Leading Δm_{31}^2 oscillations: atmospheric, CHOOZ and accelerator data

We include in our atmospheric neutrino analysis the results from the first run of Super-Kamiokande, which accumulated data during the period May 1996 to July 2001 (1489 day exposure) and is usually referred as SK-I [36], as well as the data obtained with the partial coverage after the 2001 accident (804 day exposure), the so-called SK-II period [37]. For details on the data samples and our simulation and statistical analysis we refer to the Appendix in Ref. [3]. We have not included the preliminary results of SK-III [38] (except in Fig. 7 for illustration purposes) since no oscillation analysis has been presented by the collaboration yet. For LBL accelerator experiments we combine the results on ν_μ disappearance from K2K [39] with those obtained by MINOS at a baseline of 735 km after a two-year exposure to the Fermilab NuMI beam, corresponding to a total of 3.36×10^{20} protons on target [40]. We also include the recent results on $\nu_\mu \rightarrow \nu_e$ transitions based on a exposure of 3.14×10^{20} protons on target [41].

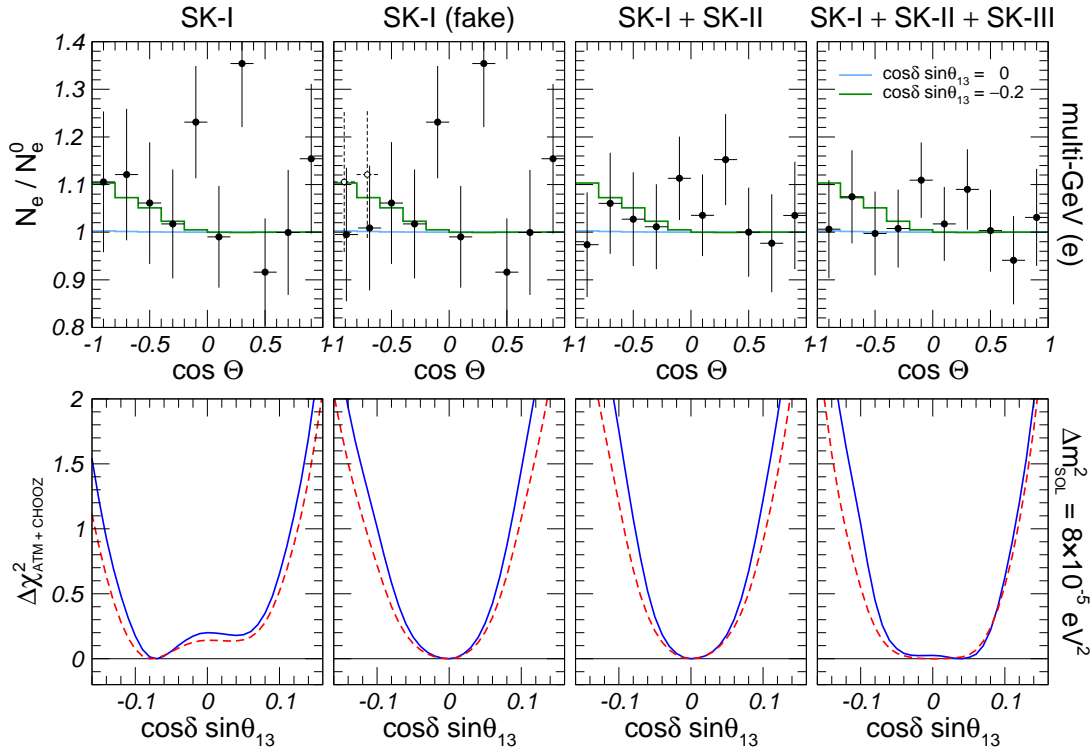


Figure 7: Zenith distribution for multi-GeV e -like events (upper panels), and $\Delta\chi^2$ dependence on $\cos\delta_{\text{CP}}\sin\theta_{13}$ (lower panels) for normal ordering (solid) and inverted (dashed). The fits include the CHOOZ data as well as the full atmospheric data samples for SK-I (left panels), SK-I with modified multi-GeV e -like data (central-left panels), SK-I + SK-II (central-right panels) and SK-I + SK-II + SK-III (right panels). Note that for consistency with the SK-III samples shown in [38] a reduced analysis with only 55 bins (instead of 90 as described in Appendix A of Ref. [24] and used through this paper) is used in all the panels of this figure.

In Fig. 6 we show the present determination of the leading parameters $|\Delta m_{31}^2|$ and θ_{23} in the limit of two-neutrino oscillations (*i.e.*, for $\theta_{13} = 0$ and neglecting the subleading effects of Δm_{21}^2) from the updated analysis of the atmospheric neutrino data and of LBL accelerator results. This figure illustrates how the bounds on the oscillation parameters θ_{23} and $|\Delta m_{31}^2|$ emerges from a complementarity of atmospheric and accelerator neutrino data: $|\Delta m_{31}^2|$ is determined by the spectral data from MINOS, whereas the mixing angle θ_{23} is still largely dominated by atmospheric data from Super-Kamiokande with a best fit point close to maximal mixing. Note the very good agreement in the location of the best fit points from both analysis. At present the sign of Δm_{31}^2 (*i.e.*, the neutrino mass hierarchy) is completely undetermined.

3.1 Impact of θ_{13} on the atmospheric and LBL ν_μ disappearance data

It is well known that a very important contribution to our knowledge of θ_{13} arises from the negative results on $\bar{\nu}_e$ disappearance at short baselines at the CHOOZ reactor experiment [42]. Given the values of Δm_{21}^2 obtained from solar and KamLAND experiments, the disappearance of $\bar{\nu}_e$ at the CHOOZ distances arises from oscillations due to $|\Delta m_{31}^2|$ whose

amplitude is proportional to $\sin^2(2\theta_{13})$. Consequently, when combined with the bounds on $|\Delta m_{31}^2|$ from atmospheric and ν_μ disappearance at LBL experiments the CHOOZ result implies an upper bound on θ_{13} .

In Ref. [11] a hint for a non-zero value of θ_{13} was obtained at 0.9σ from the analysis of atmospheric data from SK-I, ν_μ disappearance at long-baseline experiments and CHOOZ. The authors traced its origin to subleading effects driven by Δm_{21}^2 . This result was extensively studied in Ref. [10], where it was pointed out that the appearance of the hint is triggered by an excess of multi-GeV e -like data in the first two angular bins of SK-I data, which lead to a better fit for this sample in the case of a non-zero value of θ_{13} . This conclusion is summarized in Fig. 7: as clearly visible in the two leftmost panels, there is a small but definite preference for a non-zero value of θ_{13} in SK-I, however this hint disappears if the event rates for the first two bins of multi-GeV e -like events are artificially reduced by 10%. Once the SK-II data are included in the analysis the event rates of those bins are indeed reduced, and as a consequence no hint of non-zero θ_{13} is found in SK-I + SK-II and the analysis results exclusively on an upper bound θ_{13} . On the other hand, the inclusion of the preliminary SK-III seems to raise again these two bins, resulting – if not in a hint – at least in a considerable flattening of the χ^2 dependence on θ_{13} around zero. In our view, all this indicates that establishing whether a hint in favor of non-zero θ_{13} really emerges from atmospheric data is a very delicate issue, and requires an analysis with a level of accuracy which may only be achievable by the Super-Kamiokande collaboration itself.

In the lower-left panel of Fig. 4 we plot the bound on θ_{13} as implied by different combinations of atmospheric and LBL experiments. As can be seen, the bound from SK-I + SK-II data is slightly strengthened by the inclusion of LBL ν_μ disappearance data. Since the survival probability of ν_μ at the MINOS is practically insensitive to such small values of θ_{13} , this improvement can only arise as an indirect effect driven by the better determination of $|\Delta m_{31}^2|$.

3.2 $\nu_\mu \rightarrow \nu_e$ appearance results in MINOS

In Ref. [41] the MINOS collaboration reported their first results on the search for $\nu_\mu \rightarrow \nu_e$ transitions based on an exposure of 3.14×10^{20} protons-on-target in the Fermilab NuMI beam. They observe 35 events in the Far Detector with a background of $27 \pm 5(\text{stat}) \pm 2(\text{syst})$ events predicted by their measurements in the Near Detector.

In Fig. 8 we show the reconstructed energy distribution of the observed events together with the background expectations. As reported in [41] the excess of events can be well fitted under the hypothesis of $\nu_\mu \rightarrow \nu_e$ oscillations driven by a non-zero value of θ_{13} . We show in Fig. 8 our simulation of their expected spectrum in the presence of $\nu_\mu \rightarrow \nu_e$ oscillations, compared with the one given by the MINOS collaboration which show perfect agreement.

We subsequently perform an oscillation analysis of the MINOS total event rate which lead to the allowed regions shown in the right panel of Fig. 8. We show in the lower-left panel of Fig. 4 the information on θ_{13} from the analysis of the LBL data from both ν_e appearance and ν_μ disappearance and its impact when combined with the atmospheric and CHOOZ data. Altogether we find that the 1σ range for θ_{13} as determined from the

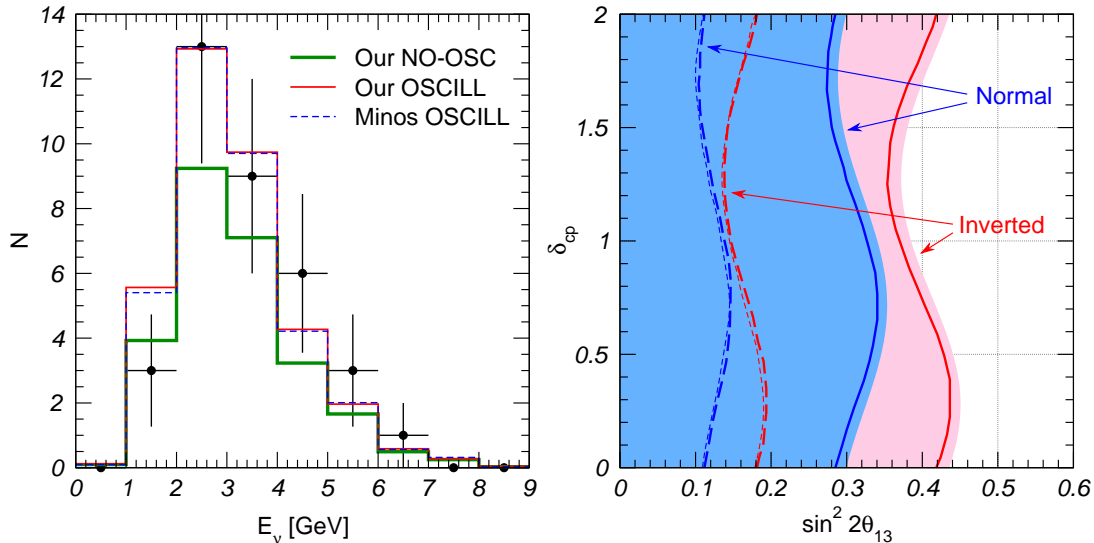


Figure 8: Left: reconstructed energy distribution of the ν_e charged current events in the MINOS far detector. We show the background prediction (thick solid green line) as well as our (red solid) and MINOS (blue dashed) predictions for the expected spectrum in the presence of $\nu_\mu \rightarrow \nu_e$ oscillations with $\sin^2 2\theta_{13} = 0.115$ and $\delta_{\text{CP}} = 0$. Right: best-fit and allowed regions for the MINOS ν_e appearance data in the δ_{CP} and $\sin^2(2\theta_{13})$ plane. The dashed (dotted) lines represent the best fit as obtained from our (MINOS) analysis for normal and inverted ordering. The solid regions are our 90% allowed regions for normal (darker blue) and inverted (lighter red); the solid lines show the corresponding regions from MINOS, taken from Ref. [43]. In both panels the remaining parameters are fixed to $\tan^2 \theta_{12} = 0.45$, maximal θ_{23} , $\Delta m_{21}^2 = 7.6 \times 10^{-5} \text{ eV}^2$ and $|\Delta m_{32}^2| = 2.43 \times 10^{-3} \text{ eV}^2$.

analysis of atmospheric, CHOOZ and LBL data reads:

$$\sin^2 \theta_{13} = 0.008_{-0.011}^{+0.016} \quad \text{ATM+CHOOZ+LBL(DIS+APP)}, \quad (3.1)$$

where to illustrate the statistical significance of $\theta_{13} = 0$ we have extrapolated the lower 1σ bound to the unphysical region $\sin^2 \theta_{13} < 0$.

4. Global results and conclusions

The results of the global combined analysis including all dominant and subdominant oscillation effects are summarized in Fig. 9, where we show the different projections of the allowed six-dimensional parameter space. The full regions correspond to the analysis done in the framework of the GS98 solar model and with Ga capture cross-section in Ref. [17] while the void regions correspond to the analysis with AGSS09 solar fluxes and the modified Ga capture cross-section in Ref. [13]. The regions in each panel are obtained after marginalization of χ_{global}^2 with respect to the undisplayed parameters. In the lower panels we show the allowed regions in the $(\sin^2 \theta_{13}, \delta_{\text{CP}})$ plane. As seen in the figure, at present the sensitivity to the CP phase is marginal but we find that the bound on $\sin^2 \theta_{13}$ can vary by about $\sim 30\%$ depending on the exact value of δ_{CP} . This arises mainly from the interference of θ_{13} and Δm_{21}^2 effects in the atmospheric neutrino observables, as well as

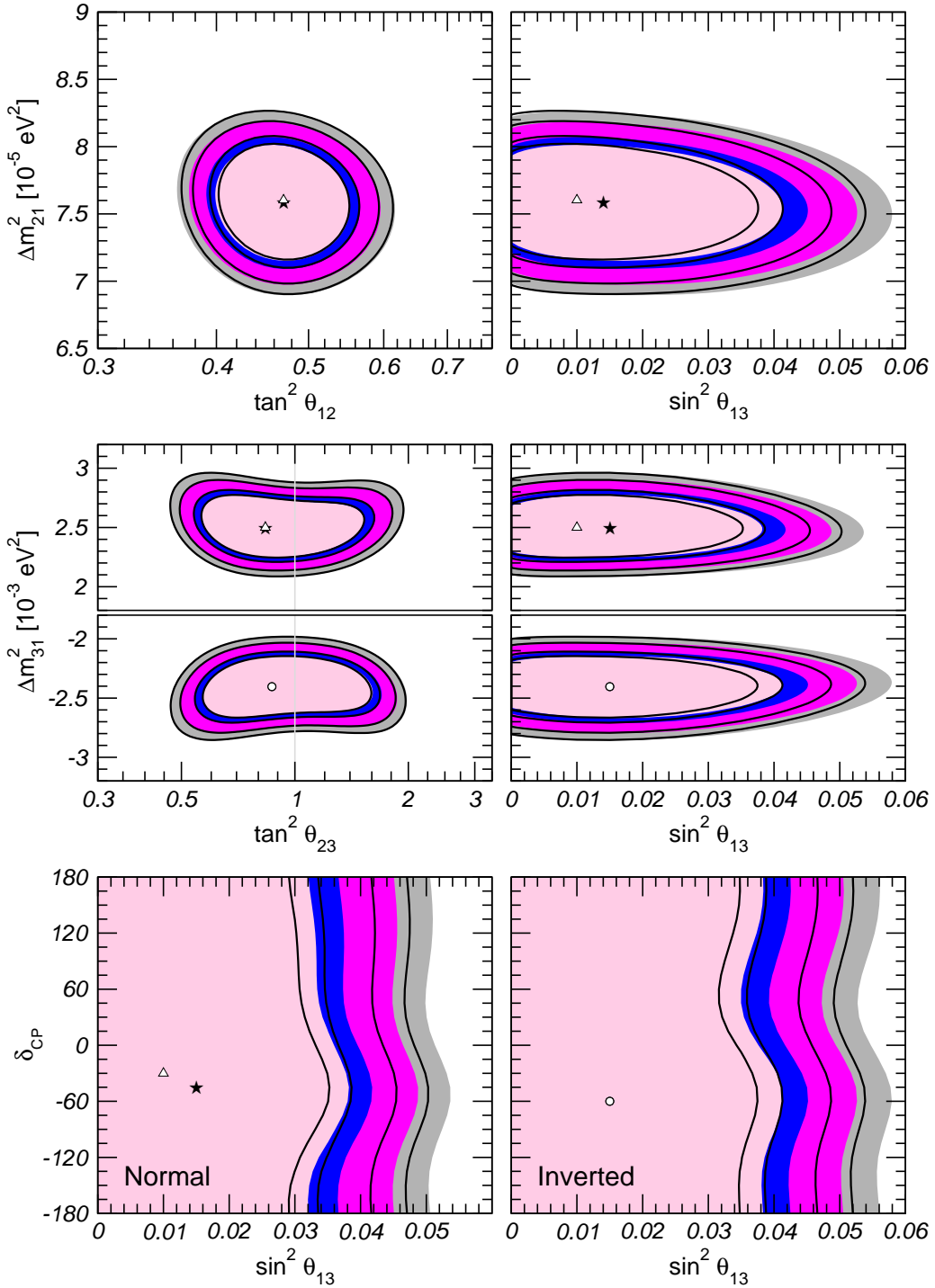


Figure 9: Global 3ν oscillation analysis. Each panels shows two-dimensional projection of the allowed five-dimensional region after marginalization with respect to the undisplayed parameters. The different contours correspond to the two-dimensional allowed regions at 90%, 95%, 99% and 3σ CL. The full regions correspond to the analysis done in the framework of the GS98 solar model and with Ga capture cross-section in Ref. [17] while the void regions correspond to the analysis with AGSS09 solar fluxes and the modified Ga capture cross-section in Ref. [13].

from the new MINOS ν_e appearance data. The derived ranges for the six parameters at the 1σ (3σ) level are:

GS98 with Gallium cross-section from [17]	AGSS09 with modified Gallium cross-section [13]
$\Delta m_{21}^2 = 7.59 \pm 0.20 \left(\begin{smallmatrix} +0.61 \\ -0.69 \end{smallmatrix} \right) \times 10^{-5} \text{ eV}^2$	Same
$\Delta m_{31}^2 = \begin{cases} -2.40 \pm 0.11 \left(\begin{smallmatrix} +0.37 \\ -0.39 \end{smallmatrix} \right) \times 10^{-3} \text{ eV}^2 \text{ (inverted)} \\ +2.51 \pm 0.12 \left(\begin{smallmatrix} +0.39 \\ -0.36 \end{smallmatrix} \right) \times 10^{-3} \text{ eV}^2 \text{ (normal)} \end{cases}$	Same
$\theta_{12} = 34.4 \pm 1.0 \left(\begin{smallmatrix} +3.2 \\ -2.9 \end{smallmatrix} \right)$	$34.5 \pm 1.0 \left(\begin{smallmatrix} +3.2 \\ -2.8 \end{smallmatrix} \right)$
$\theta_{23} = 42.3 \begin{smallmatrix} +5.3 \\ -2.8 \end{smallmatrix} \left(\begin{smallmatrix} +11.4 \\ -7.1 \end{smallmatrix} \right)$	Same
$\theta_{13} = 6.8 \begin{smallmatrix} +2.6 \\ -3.6 \end{smallmatrix} (\leq 13.2)$	$5.7 \begin{smallmatrix} +3.0 \\ -3.9 \end{smallmatrix} (\leq 12.7)$
$[\sin^2 \theta_{13} = 0.014 \begin{smallmatrix} +0.013 \\ -0.011 \end{smallmatrix} (\leq 0.052)]$	$[0.010 \begin{smallmatrix} +0.013 \\ -0.009 \end{smallmatrix} (\leq 0.049)]$
$\delta_{\text{CP}} \in [0, 360]$	Same

In summary we have presented the results of an up-to-date global analysis of neutrino oscillation data including the detailed analysis of the Borexino spectra, the lower value of Ga rate as lastly measured in SAGE, the low energy threshold analysis of the combined SNO phase I and phase II and the results for ν_e appearance from MINOS. We have studied the robustness of the hints of a non-vanishing value of θ_{13} under the inclusion of the new data and variations of the assumptions about the solar model and the possible modification of the cross-section for neutrino capture in Ga as advocated by the SAGE collaboration in order to explain their new calibration data.

We found that the inclusion of the new solar data, and in particular of the SNO-LETA results tends to lower the statistical significance of $\theta_{13} \neq 0$ while the results from ν_e appearance from MINOS increases it. Within the context of the solar model with higher metallicities (GS98) and for the original Ga capture cross-section, we conclude that the significance of $\theta_{13} \neq 0$ from solar+KamLAND data is 79% ($\Delta\chi^2 = 1.59$) which increases to 84% ($\Delta\chi^2 = 2.0$) after inclusion of the atmospheric, CHOOZ and LBL data, and in particular of the results from ν_e appearance from MINOS. We also found that using the solar neutrino fluxes required to fit the lower metallicity data (AGSS09) and/or the modified (lower) cross-section for neutrino capture in Ga lowers the best fit value of θ_{13} and its statistical significance. So when using the AGSS09 fluxes and the lower Ga cross-section the significance of $\theta_{13} \neq 0$ from solar+KamLAND data is 70% ($\Delta\chi^2 = 1.11$) and 78% ($\Delta\chi^2 = 1.53$) for atmospheric, CHOOZ and LBL data. The determination of the other oscillation parameters is rather robust.

Acknowledgments

This work is supported by Spanish MICINN grants 2007-66665-C02-01, FPA-2009-08958 and FPA-2009-09017 and consolider-ingenio 2010 grant CSD-2008-0037, by CUR Generalitat de Catalunya grant 2009SGR502, by Comunidad Autonoma de Madrid through the

HEPHACOS project P-ESP-00346, by USA-NSF grant PHY-0653342 and by EU grant EURONU.

References

- [1] B. Pontecorvo, *Neutrino experiments and the question of leptonic-charge conservation*, *Sov. Phys. JETP* **26** (1968) 984–988.
- [2] V. N. Gribov and B. Pontecorvo, *Neutrino astronomy and lepton charge*, *Phys. Lett.* **B28** (1969) 493.
- [3] M. C. Gonzalez-Garcia and M. Maltoni, *Phenomenology with Massive Neutrinos*, *Phys. Rept.* **460** (2008) 1–129, [[arXiv:0704.1800](#)].
- [4] Z. Maki, M. Nakagawa, and S. Sakata, *Remarks on the unified model of elementary particles*, *Prog. Theor. Phys.* **28** (1962) 870–880.
- [5] M. Kobayashi and T. Maskawa, *CP Violation in the Renormalizable Theory of Weak Interaction*, *Prog. Theor. Phys.* **49** (1973) 652–657.
- [6] S. M. Bilenky, J. Hosek, and S. T. Petcov, *On Oscillations of Neutrinos with Dirac and Majorana Masses*, *Phys. Lett.* **B94** (1980) 495.
- [7] P. Langacker, S. T. Petcov, G. Steigman, and S. Toshev, *On the Mikheev-Smirnov-Wolfenstein (MSW) Mechanism of Amplification of Neutrino Oscillations in Matter*, *Nucl. Phys.* **B282** (1987) 589.
- [8] G. L. Fogli, E. Lisi, A. Marrone, A. Palazzo, and A. M. Rotunno, *Neutrino masses and mixing: 2008 status*, *Nucl. Phys. Proc. Suppl.* **188** (2009) 27–30.
- [9] T. Schwetz, M. A. Tortola, and J. W. F. Valle, *Three-flavour neutrino oscillation update*, *New J. Phys.* **10** (2008) 113011, [[arXiv:0808.2016](#)].
- [10] M. Maltoni and T. Schwetz, *Three-flavour neutrino oscillation update and comments on possible hints for a non-zero θ_{13}* , [arXiv:0812.3161](#).
- [11] G. L. Fogli, E. Lisi, A. Marrone, A. Palazzo, and A. M. Rotunno, *Hints of $\theta_{13} > 0$ from global neutrino data analysis*, *Phys. Rev. Lett.* **101** (2008) 141801, [[arXiv:0806.2649](#)].
- [12] G. L. Fogli, E. Lisi, A. Marrone, A. Palazzo, and A. M. Rotunno, *SNO, KamLAND and neutrino oscillations: θ_{13}* , [arXiv:0905.3549](#).
- [13] **SAGE** Collaboration, J. N. Abdurashitov *et al.*, *Measurement of the solar neutrino capture rate with gallium metal. III: Results for the 2002–2007 data-taking period*, *Phys. Rev.* **C80** (2009) 015807, [[arXiv:0901.2200](#)].
- [14] **Borexino** Collaboration, C. Arpesella *et al.*, *Direct Measurement of the Be-7 Solar Neutrino Flux with 192 Days of Borexino Data*, *Phys. Rev. Lett.* **101** (2008) 091302, [[arXiv:0805.3843](#)].
- [15] **Borexino** Collaboration, G. Bellini *et al.*, *Measurement of the solar 8B neutrino flux with 246 live days of Borexino and observation of the MSW vacuum-matter transition*, [arXiv:0808.2868](#).
- [16] **SNO** Collaboration, B. Aharmim *et al.*, *Low Energy Threshold Analysis of the Phase I and Phase II Data Sets of the Sudbury Neutrino Observatory*, [arXiv:0910.2984](#).

- [17] J. N. Bahcall, *Gallium solar neutrino experiments: Absorption cross sections, neutrino spectra, and predicted event rates*, *Phys. Rev.* **C56** (1997) 3391–3409, [[hep-ph/9710491](#)].
- [18] B. T. Cleveland *et al.*, *Measurement of the solar electron neutrino flux with the Homestake chlorine detector*, *Astrophys. J.* **496** (1998) 505–526.
- [19] R. L. Hahn, *Radiochemical solar neutrino experiments, 'successful and otherwise'*, *J. Phys. Conf. Ser.* **136** (2008) 022003.
- [20] **Super-Kamkiokande** Collaboration, J. Hosaka *et al.*, *Solar neutrino measurements in Super-Kamiokande-I*, *Phys. Rev.* **D73** (2006) 112001, [[hep-ex/0508053](#)].
- [21] **SNO** Collaboration, B. Aharmim *et al.*, *Measurement of the ν_e and total B-8 solar neutrino fluxes with the Sudbury Neutrino Observatory phase I data set*, *Phys. Rev.* **C75** (2007) 045502, [[nucl-ex/0610020](#)].
- [22] **SNO** Collaboration, B. Aharmim *et al.*, *Electron energy spectra, fluxes, and day-night asymmetries of B-8 solar neutrinos from the 391-day salt phase SNO data set*, *Phys. Rev.* **C72** (2005) 055502, [[nucl-ex/0502021](#)].
- [23] **SNO** Collaboration, B. Aharmim *et al.*, *An Independent Measurement of the Total Active 8B Solar Neutrino Flux Using an Array of ^3He Proportional Counters at the Sudbury Neutrino Observatory*, *Phys. Rev. Lett.* **101** (2008) 111301, [[arXiv:0806.0989](#)].
- [24] M. C. Gonzalez-Garcia, M. Maltoni, and J. Salvado, *Direct determination of the solar neutrino fluxes from solar neutrino data*, [arXiv:0910.4584](#).
- [25] L. Wolfenstein, *Neutrino oscillations in matter*, *Phys. Rev.* **D17** (1978) 2369–2374.
- [26] S. P. Mikheev and A. Y. Smirnov, *Resonance enhancement of oscillations in matter and solar neutrino spectroscopy*, *Sov. J. Nucl. Phys.* **42** (1985) 913–917.
- [27] M. Asplund, N. Grevesse, and J. Sauval, *The solar chemical composition*, *ASP Conference Series* **336** (2005) 25.
- [28] M. Asplund, N. Grevesse, A. J. Sauval, and P. Scott, *The chemical composition of the Sun*, *Ann. Rev. Astron. Astrophys.* **47** (2009) 481–522, [[arXiv:0909.0948](#)].
- [29] N. Grevesse and A. J. Sauval, *Standard Solar Composition*, *Space Sci. Rev.* **85** (1998) 161–174.
- [30] J. N. Bahcall, S. Basu, M. Pinsonneault, and A. M. Serenelli, *Helioseismological Implications of Recent Solar Abundance Determinations*, *Astrophys. J.* **618** (2005) 1049–1056, [[astro-ph/0407060](#)].
- [31] W. J. Chaplin *et al.*, *Solar heavy element abundance: constraints from frequency separation ratios of low-degree p modes*, *Astrophys. J.* **670** (2007) 872–884, [[arXiv:0705.3154](#)].
- [32] S. Basu *et al.*, *Solar abundances and helioseismology: fine structure spacings and separation ratios of low-degree p modes*, *Astrophys. J.* **655** (2007) 660–671, [[astro-ph/0610052](#)].
- [33] J. N. Bahcall, A. M. Serenelli, and S. Basu, *New solar opacities, abundances, helioseismology, and neutrino fluxes*, *Astrophys. J.* **621** (2005) L85–L88, [[astro-ph/0412440](#)].
- [34] A. Serenelli, S. Basu, J. W. Ferguson, and M. Asplund, *New Solar Composition: The Problem With Solar Models Revisited*, [arXiv:0909.2668](#).
- [35] **KamLAND** Collaboration, I. Shimizu, *KamLAND (anti-neutrino status)*, *J. Phys. Conf. Ser.* **120** (2008) 052022.

- [36] **Super-Kamiokande** Collaboration, Y. Ashie *et al.*, *A Measurement of Atmospheric Neutrino Oscillation Parameters by Super-Kamiokande I*, *Phys. Rev.* **D71** (2005) 112005, [[hep-ex/0501064](#)].
- [37] P. Litchfield. Talk given at the *XXII International Conference on Neutrino Physics*, Santa Fe, New Mexico, June 13–19, 2006.
- [38] J. Raaf. Talk given at the *XXIII International Conference on Neutrino Physics*, Christchurch, New Zealand, May 25–31, 2008.
- [39] **K2K** Collaboration, M. H. Ahn *et al.*, *Measurement of Neutrino Oscillation by the K2K Experiment*, *Phys. Rev.* **D74** (2006) 072003, [[hep-ex/0606032](#)].
- [40] **MINOS** Collaboration, P. Adamson *et al.*, *Measurement of Neutrino Oscillations with the MINOS Detectors in the NuMI Beam*, *Phys. Rev. Lett.* **101** (2008) 131802, [[arXiv:0806.2237](#)].
- [41] **MINOS** Collaboration, P. Adamson *et al.*, *Search for muon-neutrino to electron-neutrino transitions in MINOS*, *Phys. Rev. Lett.* **103** (2009) 261802, [[arXiv:0909.4996](#)].
- [42] **CHOOZ** Collaboration, M. Apollonio *et al.*, *Limits on Neutrino Oscillations from the CHOOZ Experiment*, *Phys. Lett.* **B466** (1999) 415–430, [[hep-ex/9907037](#)].
- [43] M. Diwan. Talk given at the *XIII International Workshop on Neutrino Telescopes* Venice, Italy, March 10–13, 2009.